Electronic Supplementary Material (ESI) for Journal of Materials Chemistry C.

Oxidized carbon quantum dots-graphene oxide nanocomposites for improving data retention of resistive switching memory

Meng Qi,[a] Liang Bai,[b] Haiyang Xu,*[a] Zhongqiang Wang,*[a] Zhenhui Kang,[b] Xiaoning Zhao,[a] Weizhen Liu,[a] Jiangang Ma[a] and Yichun Liu[a]

[a] *Key Laboratory for UV Light-Emitting Materials and Technology (Northeast Normal University), Ministry of Education, 5268 Renmin Street, Changchun, China.*

[b] *Jiangsu Key Laboratory for Carbon-based Functional Materials and Devices, Institute of Functional Nano and Soft Materials (FUNSOM), Soochow University, Suzhou, China.*

**corresponding author.* Tel: (86)0431-85099767. E-mail: hyxu@nenu.edu.cn (Haiyang Xu); wangzq752@nenu.edu.cn (Zhongqiang Wang).

Supporting Information

The insets of Fig.S1 (a) and (b) present the surface topography of the graphene oxide (GO) film and the oxidized carbon quantum dot (OCQDs-GO) nanocomposites, as well as the corresponding AFM line profile measurements, which confirmed the thicknesses of the films to be 30 and 60 nm, respectively. The thickness of the OCQDs-GO nanocomposite was much larger than that of GO, suggesting that the OCQDs were inserted into the layered space of the GO film.

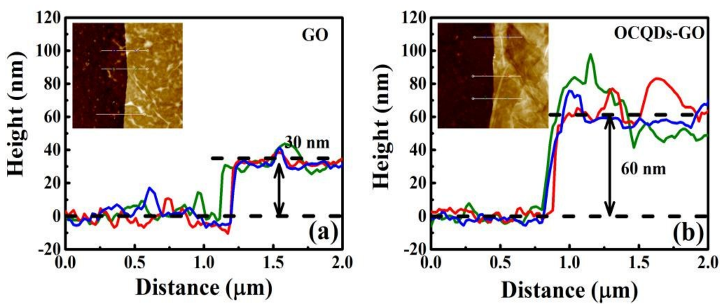

Fig.S1 (a) and (b) show the thicknesses of the GO film and the OCQDs-GO nanocomposite under the same preparation conditions, as measured using AFM.

We studied the effect of GO thickness (from 30 to 60 nm) on the RS characteristics of the GO-based RRAM device. The high/low resistance states (HRS/LRS), set/reset voltages (V_{set}/V_{reset}), and forming voltages were compared in our experiments, as shown in Fig.S2 (a) and (b). There is no obvious dependence of HRS/LRS and

V_{set}/V_{reset} for different GO thicknesses; however, the forming voltage clearly increased from 2.3 (30 nm) to 4 V (60 nm). We further studied these devices when applying a small CC of 500 μA (Fig.S2 (c)); the results show that the volatile switching behaviors are still observable regardless of the GO thickness. In addition, as seen in Fig.S2 (d), the activation energy (E_a) of the devices with different GO thicknesses were almost the same, with an acceptable margin of error. Therefore, we can conclude from the above-mentioned experimental results that the GO thickness has no obvious effect on the RS performance (apart from the forming voltages).

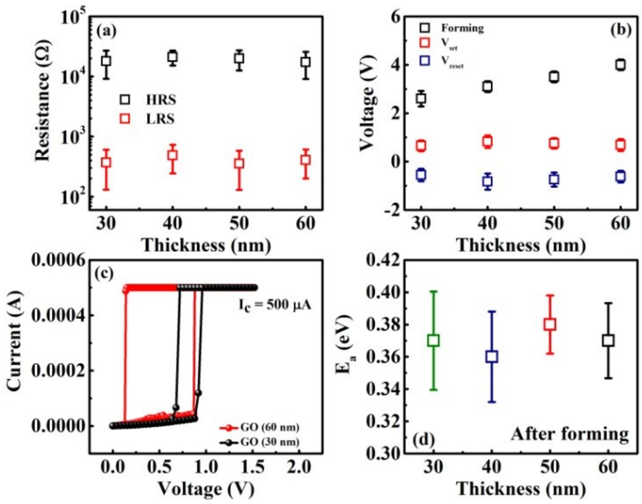

Fig.S2 Comparison of (a) the HRS/LRS characteristics and (b) $V_{forming}$, V_{set} and V_{reset} for GO samples with different thicknesses. (c) The RS behaviors of films with different thicknesses (30 and 60 nm) at a CC of 500 μA. (d) The activation energy for the GO samples with different thicknesses.

Fig.S3 (a) presents the bipolar RS curves of Al/unoxidized CQDs (UCQDs)-GO/ITO memory, which were measured in voltage sweep mode using a Keithley 2636A Source Meter under vacuum. Herein, we define that the positive current flows from the top to the bottom electrode, and a compliance current (CC) of 500 μA was set to protect the device from hard breakdown. Fig.S3 (b) shows that the averaged values of V_{set}/V_{reset} remain almost constant as the UCQDs concentration is increased, which means that no more C-O-C groups were introduced. Fig.S3 (c) illustrates that the HRS clearly decreased along with the UCQD concentration, resulting in the shrinkage of the switching window. Fig.S3 (d) shows the retention characteristics of the HRS and LRS with different UCQDS concentrations (4.5, 8.5, 18.5, and 31.5 wt%) in the Al/UCQDs-GO/ITO device, and all those resistance states were retained for 10^4 s without any degradation. The decrease of HRS means that the devices is unable to be operated under much lower CC.

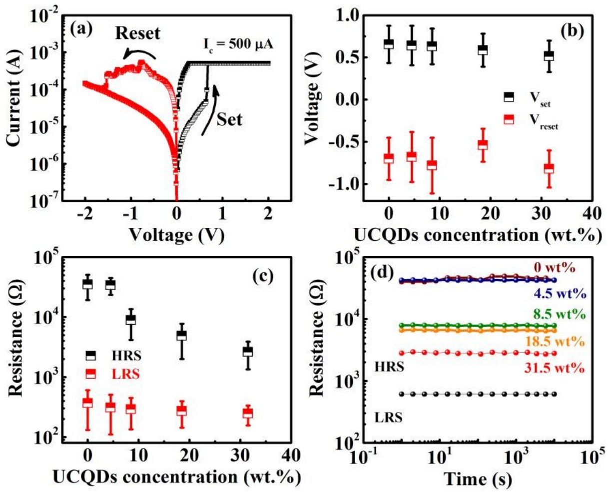

Fig.S3 (a) shows the RS behavior of an Al/UCQDs-GO/ITO device under a CC of 500 μA. Panels (b) and (c) show the averaged values of V_{set}/V_{reset} and the variations of HRS/LRS with different concentrations of UCQDs, respectively. (d) The retention time of the HRS and LRS of Al/UCQDs-GO/ITO devices with different concentration of the UCQDs.

Both the increase of E_a and the increase of the oxygen defect density in a single filament (CF) can improve the LRS retention. Based on our experimental results, embedding OCQDs into GO may be an effective method to increase E_a, while embedding unoxidized CQDs may be capable of enhancing the oxygen defect density in a single CF. As shown in Fig.S4 (a), the E_a of the devices with the embedded unoxidized CQDs was almost constant at 0.36 eV. Meanwhile, the E_a increased from 0.37 to 0.78 eV as the OCQDs concentration was increased. Thus, the embedding of OCQDs or unoxidized CQDs may improve LRS robustness in two different ways. However, the decrease of HRS with embedding unoxidized CQDs means that the devices are unable to be operated under a much lower CC (Fig.S4 (b)). The real switching ratio is likely even lower if switching fluctuations are taken into account; to obtain a good performance, the study of embedding unoxidized CQDs was not carried out in this work.

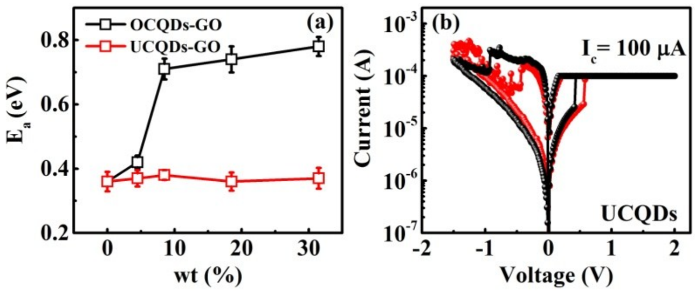

Fig.S4 (a) The dependence of E_a on the embedded concentration of OCQDs and UCQDs, respectively. (b) The RS behavior of the device with the embedded UCQDs at 100 μA.

The electrical measurements were conducted under vacuum using an Agilent B1500A semiconductor analyzer and a cryogenic probe station (Lake Shore, TTPX). These instruments can characterize the devices in a voltage sweep module for DC measurements; for pulse operation to probe the switching time we used the Keysight Technologies Waveform Generator/Fast Measurement Unit (WGFMU) module. The compliance current used was the default setting for the Agilent B1500A. The test switching time was also obtained with the WGFMU module (from the manual of Keysight Technologies B1500A Waveform Generator/Fast Measurement Unit), the schematic diagram of which is shown in Fig.S5 (a). When measuring a two-terminal device, channel 1 applies pulses to the devices and channel 2 monitors the current response in the devices. Thus, these two signals correspond directly to the input and output signals in our measurements (Fig.S5 (b)).

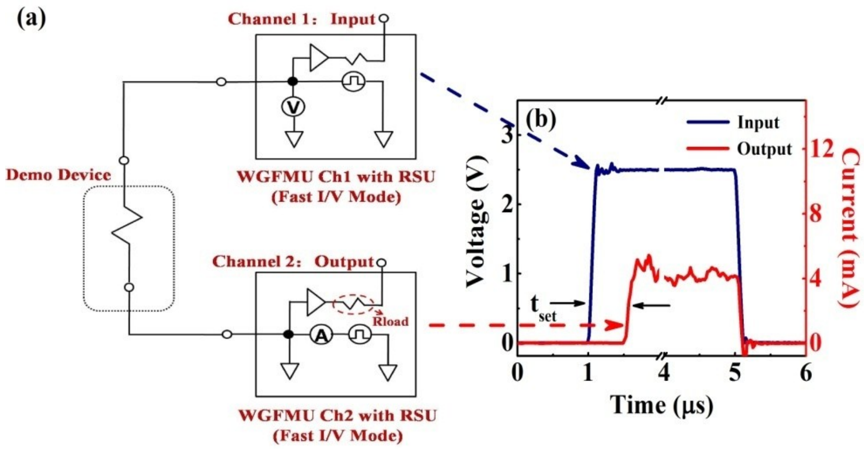

Fig.S5 (a) shows the schematic diagram of the Agilent B1500A. (b) Typical response profiles of the t_{set} measurement.

The TEM image of the OCQDs was shown the Fig.S6 (a); examining the diameters of the OCQDs yielded that they were in the range of 2–6 nm (Fig.S6 (b)).

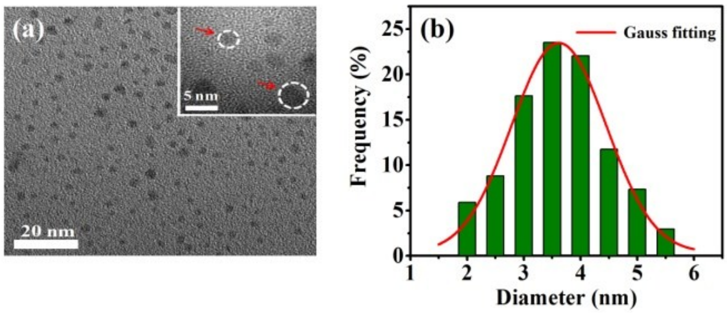

Fig.S6 TEM images of (a) the OCQDs. (b) The Histogram of OCQDs size distribution.

We have studied the relationship of the migration energy barrier E_a for different concentrations of OCQDs, as shown in Fig.S7. Fig.S7 (a), (d), and (g) illustrates the switching response of the Al/OCQDs-GO/ITO device for various OCQDs concentrations (4.5, 18.5, and 31.5 wt%) at different temperatures by applying voltage pulses (2.5 V/4 μs). It can be clearly observed that the switching time (t_{set}) decreases as for all these devices as the temperature increases; these data are also statistically displayed in Fig.S7 (b), (e), and (h). Furthermore, using the temperature-accelerated Arrhenius law, the E_a values were calculated and compared by extracting the slope of the Arrhenius plots, as shown in Fig.S7 (c), (f), and (i). Adding these E_a values to previous data, it can be observed that the E_a clearly increased from 0.37 to 0.78 eV with increasing OCQDs concentration (from 0 to 31.5 wt%). Therefore, the above results confirm that the embedded OCQDs are responsible for the increase of E_a in this study.

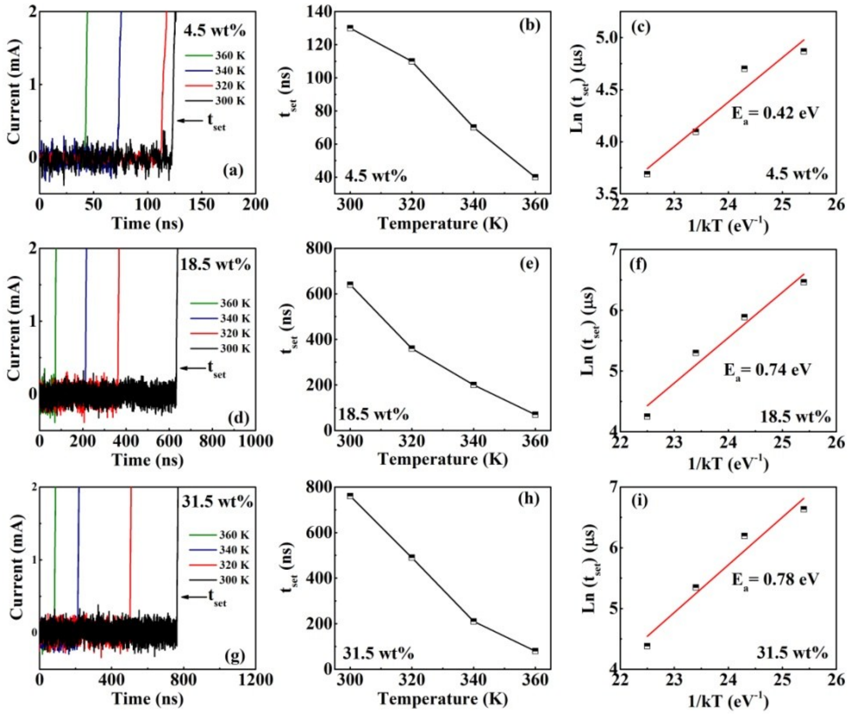

Fig.S7 The switching responses of the devices with different OCQD concentrations, i.e., (a) 4.5, (b) 18.5, and (c) 31.3 wt%, at different temperatures. Panels (b), (e), and (h) show the dependence of t_{set} on the temperature for 4.5, 8.5, and 31.3 wt% OCQDs loading, respectively. Panels (c), (f), and (i) show the Arrhenius fitting plots for the devices with 4.5, 8.5, and 31.3 wt% OCQDs loading, respectively.

Reference:

[1] S. Choi, J. Lee, S. Kim and W. D. Lu, Retention failure analysis of metal-oxide based resistive memory, Appl. Phys. Lett., 2014, 105(11), 113510.